Surface Acidity and Basicity of La_2O_3, LaOCl, and $LaCl_3$ Characterized by IR Spectroscopy, TPD, and DFT Calculations

Olga V. Manoilova,[+] Simon G. Podkolzin,[‡] Balarishna Tope,[§] Johannes Lercher,[§] Eric E. Stangland,[‡] Jean-Michel Goupil,[#] and Bert M. Weckhuysen*,[+]

Departement Anorganische Chemie en Katalyse, Debye Instituut, Universiteit Utrecht, Sorbonnelaan 16, 3584 CA Utrecht, The Netherlands, Core Research and Development, The Dow Chemical Company, Midland, Michigan 48674, Laboratory "Catalyse et Spectrochimie", UMR CNRS, ENSICAEN, Caen University, 6 bd. Maréchal Juin, 14050 Caen Cedex, France, and Institute for Chemical Technology, Technische Universität München, Lichtenbergstrasse 4, D-85747 Garching, Germany

Received: April 23, 2004; In Final Form: July 6, 2004

Adsorption sites of La_2O_3, LaOCl, and $LaCl_3$ catalysts were characterized with probe molecules using infrared spectroscopy, temperature-programmed desorption (TPD), and density-functional theory (DFT) calculations. Surface acid sites were probed with CO, pyridine, and 2,6-dimethylpyridine (DMP), and basic sites were probed with CO_2. Shifts of the CO vibrational frequency at low surface coverage at 77 K suggest that the strength of Lewis acid sites increases with the concentration of Cl in the material; i.e., La_2O_3 < LaOCl < $LaCl_3$. DFT estimates for CO adsorption energies and LUMO energies were consistent with this ranking. On the basis of a downward shift of the surface OH stretching bands interacting with CO, pyridine, and DMP spectra at room temperature (RT) and TPD results, and confirmed by DFT calculations, the strength of Brønsted acid sites was concluded to increase in the same order. Additional DFT calculations with a frequency analysis were used to elucidate CO_2 adsorption modes. DFT calculations and IR spectra of CO_2 adsorbed on LaOCl suggest that CO_2 forms coupled bridged species. Proton affinity calculations were used to rank the basicity strength of surface O and Cl sites. The amount of CO_2 adsorbed on $LaCl_3$ was negligibly small, confirming the requirement of lattice O adsorption sites. IR spectra of CO_2 adsorbed on La_2O_3 at RT were similar to those of bulk $La_2(CO_3)_3$ and, accordingly, were assigned to the formation of polydentate and bulk carbonates. CO_2 evolution from La_2O_3 in TPD experiments closely matched the reported thermal stability of $La_2(CO_3)_3$.

Introduction

La_2O_3, LaOCl, and $LaCl_3$ are important catalytic materials that are actively studied for many hydrocarbon-conversion applications both as supports and as supported or self-supporting active components. For example, catalysts based on La_2O_3 and LaOCl were investigated for methane coupling[1−4] and for ethane oxidative dehydrogenation.[5,6] $LaCl_3$ was shown to be a promising catalyst for methane oxidative chlorination[7] and for converting ethane to vinyl chloride in a single step.[8,9]

Our group studied both catalytic and noncatalytic decomposition of C_1 chlorinated hydrocarbons over La_2O_3, LaOCl, and $LaCl_3$ materials and found that the extent of the surface and bulk chlorination changed dynamically with reaction conditions.[10−13] In addition, the degree of chlorination was found to have a dramatic effect on catalytic activity. These changes in the acid−base properties could be related to global properties of the material related to the average electronegativity of the material and/or to specific changes in the acidic and basic sites on the surface, which can be both characterized by interaction with probe molecules. Here, we use CO, pyridine, and 2,6-dimethylpyridine (DMP) for acidic sites and CO_2 for basic sites characterizing the interactions with infrared spectroscopy (IR), temperature-programmed desorption (TPD), and density-functional theory (DFT) calculations. The choice of CO and CO_2 is particularly useful because these gases are usually formed during hydrocarbon reactions and, as a result, the elucidation of their adsorption modes should be helpful in understanding the mechanisms of these reactions. Furthermore, since there have been repeated efforts for acidity−basicity systematization based on probe molecule characterization of metal oxides (for example[14,15]), the results of this work should contribute to the classification of La_2O_3, LaOCl, and $LaCl_3$ relative to the numerous previously characterized solids.

The choices of probe molecules for characterizing acid−base surface sites have been extensively discussed, and each probe has its own advantages and limitations.[14,16,17] CO is a weak electron donor that is extensively used for probing the surface acidity of metal oxides.[14,18,19] It should be emphasized here, however, that the extent of a surface interaction with CO depends not only on the electron-acceptor (acidic) properties of the adsorption site but also on the local availability of d electrons allowing back-donation into the antibonding π orbital of CO. Without available d electrons, adsorption of CO on Lewis acid sites increases the wavenumber of the CO stretching vibration in proportion to the intensity of the interaction. This results in a stronger shift for adsorption on metal cations and a weaker shift for adsorption on OH groups. The relative concentration of the sorption sites is provided by the relative intensity of the bands. The perturbation of OH frequencies to lower wavenumbers is usually significant and can serve as a

* Author to whom correspondence should be addressed. E-mail: b.m.weckhuysen@chem.uu.nl.
[+] Universiteit Utrecht.
[‡] The Dow Chemical Company.
[#] Caen University.
[§] Technische Universität München.

10.1021/jp040311m CCC: $27.50
Published on Web 09/15/2004

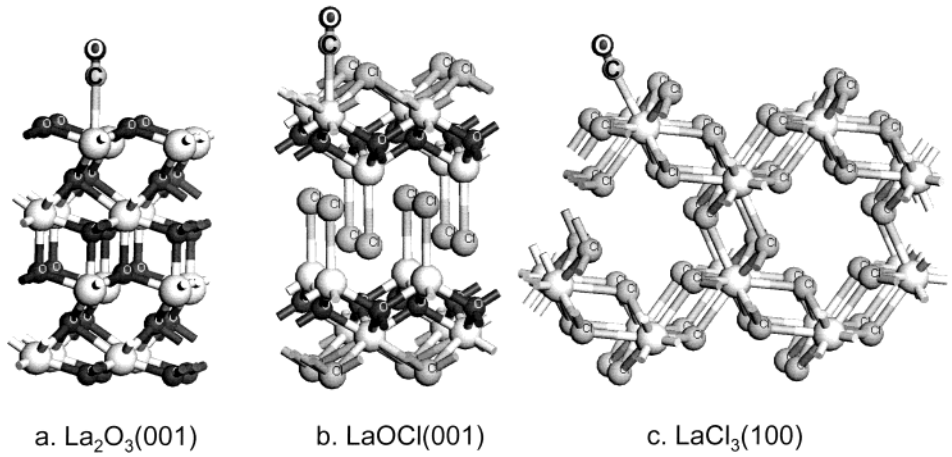

Figure 1. CO adsorption on Lewis acid sites of model surfaces. One unit cell for each periodic structure is shown.

measure of Brønsted acidity for electron-accepting sites. Pyridine and DMP are more basic than CO, their respective proton affinities (PA) being 930, 963, and 594 kJ/mol.[20] As a consequence, pyridine and DMP differentiate stronger between acidic sites and can serve as highly sensitive probes of Brønsted acidity on the basis of the formation of the corresponding protonated species with characteristic ν_{8a} and ν_{8b} vibrational bands in the 1670−1620 cm^{-1} region.[17,21−24] CO_2 is widely used for testing surface basicity.[16,17] On reaction with basic surface oxygen, different types of carbonates are formed, which, in conjunction with their thermal stability, are used for basicity discrimination.

In the present paper, we address this question by combining DFT calculations and surface site characterization with CO, pyridine, dimethyl pyridine, and CO_2 using in situ infrared spectroscopy and TPD as primary analytical tools.

Experimental Section

Catalyst Preparation and Characterization. Commercial La_2O_3 and $LaCl_3 \cdot 7H_2O$ (99.99%, Acros Organics, Inc.) with specific surface areas of about 1 m^2/g were used as starting materials. LaOCl samples were prepared by precipitation using $LaCl_3$, $La(NO_3)_3 \cdot 6H_2O$ (98+%, Acros Organics, Inc), commercial NH_4OH, and HCl. The gel was dried at 390 K and then calcined at 820 K. XRD showed the phase purity of LaOCl. The surface area determined by N_2 sorption was around 45 m^2/g. $La_2(CO_3)_3 \cdot H_2O$ (99.9%) was purchased from Sigma-Aldrich Inc.

Infrared Spectroscopy. Infrared spectra were collected using Nicolet 710 and Bruker Tensor 27 spectrometers with a resolution of 4 cm^{-1}. Two IR cells were used: (1) a glass cell for room temperature (RT) measurements and (2) a low-temperature stainless steel cell described previously.[25] The latter cell was equipped with crystalline ZnSe inner windows, which, in combination with the outer KBr windows, allowed us to collect spectra in the region of 4000−500 cm^{-1} at 77−300 K. All low-temperature spectra were recorded in the presence of 0.5−1.3 mbar of He in the inner volume of the cell. The purity of materials was 99.995%: CO and CO_2 were from Air Liquid, Inc. (99.9%); pyridine and 2,6-dimethylpyridine (DMP) were from Sigma-Aldrich, Inc. (99+%).

Samples (about 20 mg) were pressed into self-supported 2 cm^2 disks and activated in situ prior to IR measurements. The La_2O_3 sample was calcined for several hours in oxygen and then in a vacuum at 1070 K. For CO adsorption, additional spectra were collected with the La_2O_3 sample pretreated at 770 K. The LaOCl samples were pretreated in a vacuum at 820 K. The $LaCl_3 \cdot 7H_2O$ sample was heated at a rate of 1 K/min to 820 K and held at this temperature for 10 h. The dehydration of $LaCl_3$ was verified spectroscopically by the absence of adsorbed water bands. Before adsorbate introduction, the samples were cooled to the corresponding experimental temperatures under a vacuum of 5×10^{-5} mbar.

CO was initially dosed at 77 K up to the equilibrium pressure of 10.6 mbar. The gas was then evacuated in sequential steps for studying the coverage dependence. After every evacuation step, some He was added for a better sample temperature control. DMP and pyridine were dosed at RT up to the equilibrium pressure of 1.3 mbar. The gas was then progressively evacuated at RT and then at elevated temperatures up to 470K. CO_2 adsorption was performed by admitting small doses at RT up to the final equilibrium pressure of 1.3 mbar.

Temperature-Programmed Desorption. Temperature-programmed desorption (TPD) experiments with DMP and CO_2 were performed in a tubular reactor under He flow with the effluent analyzed by a Balzers QMG 420 mass spectrometer. The heating rate was 10 K/min, and the sampling frequency was 1 min^{-1}. Solid samples (~200 mg) were initially degassed by evacuation to $\sim 10^{-3}$ mbar and then treated by heating at 10 K/min to 773 K (1073 K for La_2O_3) and holding at this temperature for 1 h. After being cooled to 303 K, the samples were equilibrated with ~1 mbar of a probe gas for 1 h and then evacuated to 1.3×10^{-3} mbar for 1 h.

Density Functional Theory Calculations. Gradient-corrected periodic DFT calculations with La_2O_3, LaOCl, and $LaCl_3$ model surfaces were performed using the DMol3 code in Materials Studio 2.2 software by Accelrys, Inc. Infinite slabs were constructed similarly to our recently reported La_2O_3(001) model used in the elucidation of the CCl_4 decomposition mechanism.[10] The models were based on a 2×2 La unit cell with the overall thickness of 10 layers, as shown in Figure 1. The bottom three slab layers were constrained during the calculations, and the top six layers were optimized with an adsorbate, simulating surface relaxation on adsorption. All adsorption and surface reaction energies were calculated at 0 K without zero-energy corrections. The calculations used the double numerical with polarization (DNP) basis set and the generalized gradient-corrected Perdew−Wang (GGA PW91) functional. The calculations were spin nonpolarized except for proton affinity calculations. Tightly bound core electrons were represented with semi-core pseudopotentials. Reciprocal-space integration over the Brillouin zone was approximated through k-point sampling

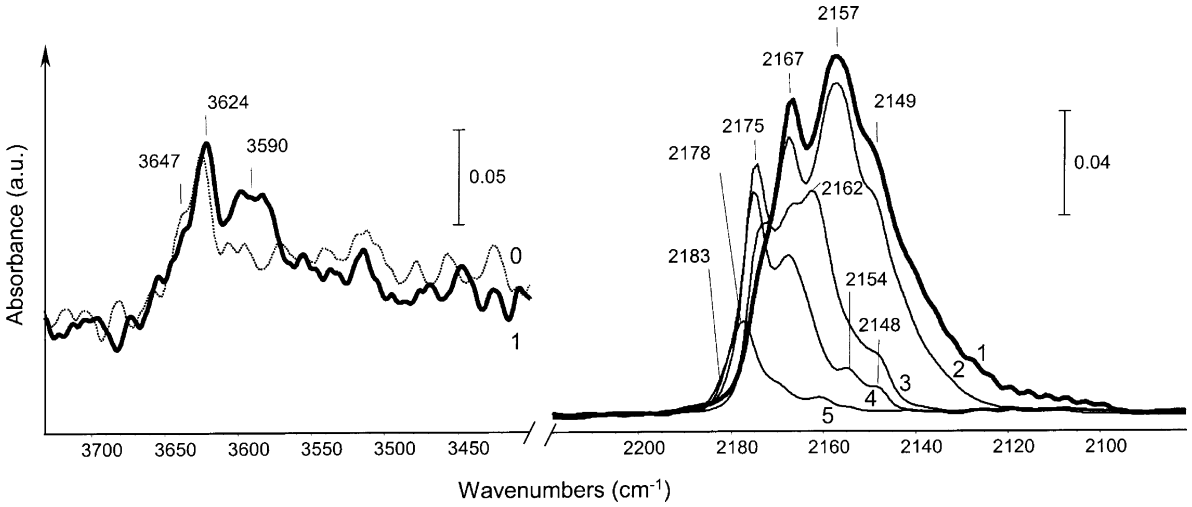

Figure 2. FTIR spectra of CO adsorbed at 77 K on La_2O_3 pretreated at 1070 K: 0, before adsorption; 1, after admission of 10.6 mbar CO in equilibrium; 2, after evacuation of gas-phase CO to 1.3×10^{-4} mbar; 3, after evacuation for 3 min at 1.3×10^{-4} mbar; 4, after evacuation for 5 min at 1.3×10^{-5} mbar; 5, after evacuation for 7 min at 1.3×10^{-5}; and 6, after evacuation for 15 min at 1.3×10^{-5} mbar. Spectrum 0 was subtracted in the CO spectral region.

with a separation of 0.05 1/Å using the Monkhorst−Pack grid: La_2O_3 ($3 \times 3 \times 1$), LaOCl ($2 \times 2 \times 1$), and $LaCl_3$ ($1 \times 2 \times 1$). Convergence with respect to the number of k-points was tested by decreasing the k-point separation distance to 0.04 1/Å for representative structures. For geometry optimization, the energy convergence criterion was set at 0.025 kJ/mol. The usually stated accuracy of DFT calculations for predicting adsorption energies is about 20 kJ/mol. Since this accuracy value depends on the validity of the employed surface model, our computational results were interpreted mostly in terms of relative trends by comparing different models, rather than in terms of absolute values for a single model. The calculated equilibrium lattice constants closely matched accepted experimental values: $a = b = 3.954$ (experimental 3.939), $c = 6.136$ (6.136) Å for La_2O_3; $a = b = 4.150$ (4.109), $c = 6.875$ (6.865) Å for LaOCl; and $a = b = 4.351$ (4.375), $c = 7.621$ (7.478) Å for $LaCl_3$.

For geometry optimization, the energy convergence criterion was set at 0.025 kJ/mol. The usually stated accuracy of DFT calculations for predicting adsorption energies is about 20 kJ/mol. Since this accuracy value depends on the validity of the employed surface model, our computational results were interpreted mostly in terms of relative trends by comparing different models, rather than in terms of absolute values for a single model. The calculated equilibrium lattice constants closely matched accepted experimental values: $a = b = 3.954$ (experimental 3.939), $c = 6.136$ (6.136) Å for La_2O_3; $a = b = 4.150$ (4.109), $c = 6.875$ (6.865) Å for LaOCl; and $a = b = 4.351$ (4.375), $c = 7.621$ (7.478) Å for $LaCl_3$.

Model surfaces were selected by considering multiple cleavage options for low-index crystal planes: (001), (100), (110), and (111). All evaluated unit cells were created to preserve the overall bulk stoichiometry of the materials. In agreement with previous experimental and theoretical studies,[26−29] the (001) plane terminated with oxygen was identified as the most energetically stable one for La_2O_3. Chlorine-terminated LaOCl(001) and $LaCl_3$(100) were identified as the lowest-energy surface models for the respective materials. Other considered crystal planes and surface terminations were less energetically favorable by 15−80 kJ/mol. Our reported activity results for CCl_4 decomposition over LaOCl surfaces, characterized by X-ray photoelectron spectroscopies, demonstrate that terminal lattice oxygen is usually present in addition to chlorine.[10,13] To probe adsorption properties of such mixed surfaces, an additional model for LaOCl(001) was generated by substituting two terminal Cl atoms with one O atom, creating a mixed O−Cl-terminated surface. A vacuum spacing of 15 Å was used in all surface models. Frequency calculations were performed with a partial Hessian, using only the adsorbate and the bonding lattice atoms. Including all top-layer surface atoms in the frequency calculations for several representative structures had a small effect on the results: the differences were within 5 cm^{-1}.

Results and Discussion

1. Surface Acidity. *1.1. CO Adsorption.* Prior to CO adsorption, the initial FTIR spectrum of La_2O_3 pretreated at 1070 K exhibited a single weak ν(OH) band at 3624 cm^{-1} with a shoulder at 3647 cm^{-1}, as shown in spectrum 0 of Figure 2. This has been attributed to bridged La−OH groups, type II.[30] After equilibration with 10.6 mbar of CO at 77 K, the band of the free hydroxy groups was only slightly perturbed, generating a perturbed OH band at 3590 cm^{-1} (see spectrum 1 in Figure 2 and Table 1). The intensity of the band at 3624 cm^{-1} was almost unchanged, and the shoulder at 3647 cm^{-1} disappeared. When the sample was calcined at 770 K, a single OH band appeared at 3644 cm^{-1}, which led to a perturbed hydroxy band at 3604 cm^{-1} after CO addition.

In the ν(CO) spectral region, bands at 2157 cm^{-1} with a shoulder at 2149 cm^{-1}, and at 2167 cm^{-1} with a shoulder at 2175 cm^{-1} (see spectrum 1 in Figure 2), were observed after pretreatment at 1070 K. With the sample pretreated at 770 K, three bands were observed at 2133, 2155, and 2165 cm^{-1}. During evacuation, the intensity of the band at 2157 cm^{-1} was reduced significantly and the shoulder at 2175 cm^{-1} became a separate band with a shoulder at 2183 cm^{-1} (spectrum 5 in Figure 2). These latter two peaks are previously attributed to CO adsorbed on La^{3+} sites.[31]

The spectrum of the activated LaOCl (see spectrum 0 in Figure 3) had an intense free hydroxyl band at 3634 cm^{-1} and a weaker one at 3624 cm^{-1}. After CO adsorption, the band at 3634 cm^{-1} shifted −58 cm^{-1} down to 3576 cm^{-1} (see spectrum 1 in Figure 3 and Table 1). This new OH band is attributed to hydrogen-bonded CO with hydroxy groups of La_2O_3. In agreement with this interpretation, the shoulder at 2155 cm^{-1} (close to the C−O vibration of free CO) disappeared first,

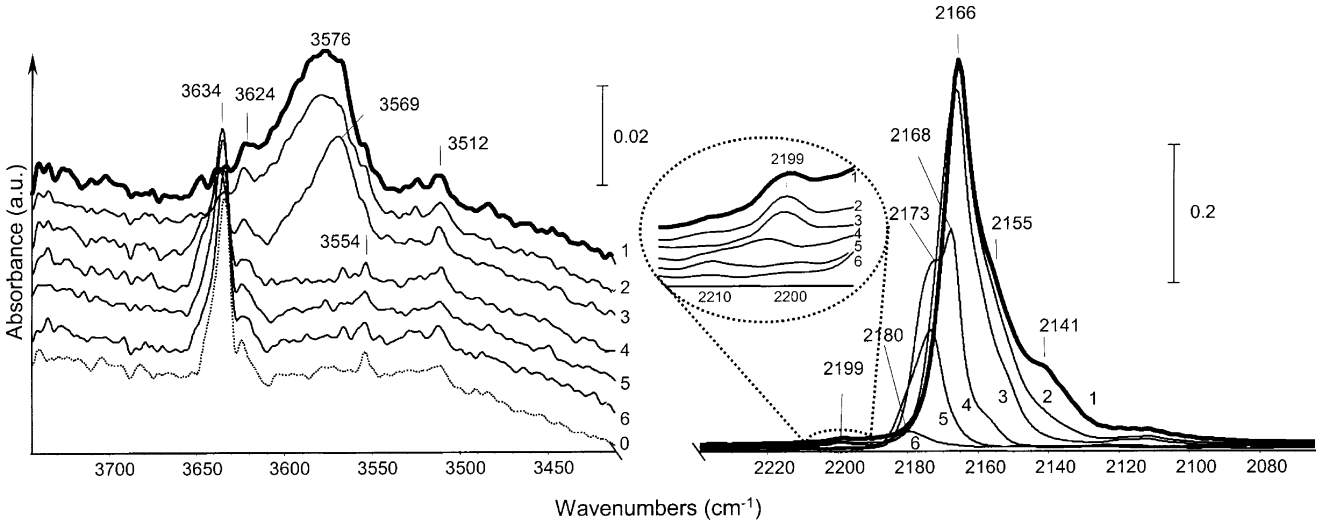

Figure 3. FTIR spectra of CO adsorbed at 77 K on LaOCl pretreated at 820 K: 0, before adsorption; 1, 10.6 mbar CO in equilibrium; 2, evacuation of gas-phase CO to 1.3×10^{-4} mbar; 3, evacuation for 30 s at 1.3×10^{-4} mbar; 4, evacuation for 5 min at 1.3×10^{-5} mbar; 5, evacuation for 15 min at 1.3×10^{-5} mbar; and 6, evacuation for 20 min at 1.3×10^{-5} mbar. Spectrum 0 was subtracted in the CO spectral region.

TABLE 1: Evaluation of Brønsted Acid Sites on La_2O_3, LaOCl, and $LaCl_3$

	La_2O_3	LaOCl	$LaCl_3$
$\Delta\nu$(OH) experimental at high CO coverage, cm^{-1}	−34	−58	−107
computational model surface	La_2O_3(001)	LaOCl(001) Cl-only	$LaCl_3$(100)
$\Delta\nu$(OH) calculated with H-bonded CO, cm^{-1}	no comparable surface OH model	−38	−107
ΔE for OH^- (surf) = O^{2-}(surf) + H^+ at 0.25 ML, kJ/mol		1702	1524

suggesting even weaker interactions.[19] The original hydroxyl band at 3634 cm^{-1} was restored after prolonged evacuation (spectra 4−6 in Figure 3), indicating that the interaction with the hydroxy groups is very weak. The shoulder at 2141 cm^{-1} is attributed to physisorbed species. The main peak at high coverage was at 2166 cm^{-1}. There was an additional small band at 2199 cm^{-1} (spectrum 1 in Figure 3). On evacuation, the main peak shifted to 2168 cm^{-1} and developed a shoulder at 2173 cm^{-1} (spectrum 4 in Figure 3). Additional evacuation shifted this peak further to 2180 cm^{-1} and the peak at 2199 cm^{-1} to 2208 cm^{-1} (spectrum 6 in Figure 3).

The spectrum of $LaCl_3$ pretreated at 820 K showed ν(OH) bands at 3735 cm^{-1} (weak), and at 3635 cm^{-1} (broad) with a shoulder at 3658 cm^{-1}, and two more broad bands at 3587 and 3485 cm^{-1} (spectrum not shown). It is not common to observe hydroxy groups on surfaces of chlorides. As $LaCl_3$ is very hygroscopic, these OH bands are attributed to water molecules coordinated on the surface. This explanation is supported by a low-intensity δ(HOH) band at 1610 cm^{-1}. After CO admission, a weak band of perturbed hydroxy groups was observed only in the difference spectra. The OH bands at 3658 and 3587 cm^{-1} disappeared, and a broad band appeared at 3480 cm^{-1} (spectrum 1 in Figure 4). This shift corresponds to a downward shift of the ν(OH) of −178 cm^{-1} (Table 1).

Similar to the observation of H-bonded CO on LaOCl, a shoulder at 2155 cm^{-1} was observed. In analogy, this shoulder disappeared and the ν(OH) bands were restored on evacuation (spectra 3−6 in Figure 4). At high coverage, physisorbed CO was observed at 2140 cm^{-1}; also, with $LaCl_3$, the main chemisorption peak was at 2166 cm^{-1} with an additional small peak at 2200 cm^{-1} (spectrum 1 in Figure 4). The only salient difference between LaOCl and $LaCl_3$ at high CO coverage was a well-defined shoulder at 2179 cm^{-1} for $LaCl_3$. On evacuation, the main peak at 2166 cm^{-1} diminished rapidly, and its shoulder at 2179 cm^{-1} became the dominant feature shifting to 2184 cm^{-1} (spectra 2−6 in Figure 4).

For DFT calculations, surface models of Brønsted acid sites for LaOCl(001) and $LaCl_3$(100) were generated by substituting one terminal Cl atom by an OH group in the unit cells shown in Figure 1. For the $LaCl_3$ model, multiple OH positions were evaluated, and the most energetically favorable one was selected. CO was then positioned above the terminal hydroxyls, and the geometries were optimized. The resulting structures are presented in Figure 5. The adsorption energies for the two models are similar: −12 to −14 kJ/mol. However, the calculated C···H bond distance is slightly smaller for $LaCl_3$: 2.27 versus 2.29 Å. This difference translates to a bigger predicted change in the OH vibrational frequency on CO adsorption for $LaCl_3$: −107 versus −38 cm^{-1} (Table 1). The magnitude of these values and the trend are consistent with the values determined experimentally by IR spectroscopy, i.e., −102 and −58 cm^{-1}. This trend suggests that OH groups are more acidic on $LaCl_3$. The DFT results for the H-bonded CO are very sensitive to the initial geometry chosen because the interactions are weak. Therefore, an additional measure of hydroxyl acidity was employed for quantifying differences between the models. Proton affinity (PA) was chosen as a descriptor because it predicts bigger energy differences, which are better described by DFT, and provides an acidity measure independent of a probe molecule.[32,33] The calculated proton abstraction energies for the LaOCl and $LaCl_3$ models in Figure 5 were, respectively, 1702 and 1524 kJ/mol (Table 1). This result shows that it is easier to abstract H^+ from OH on $LaCl_3$, and therefore, this surface is predicted to have stronger Brønsted acid sites.

The experimentally observed changes in ν(OH) upon CO adsorption, which were −34, −58, and −107, respectively, for

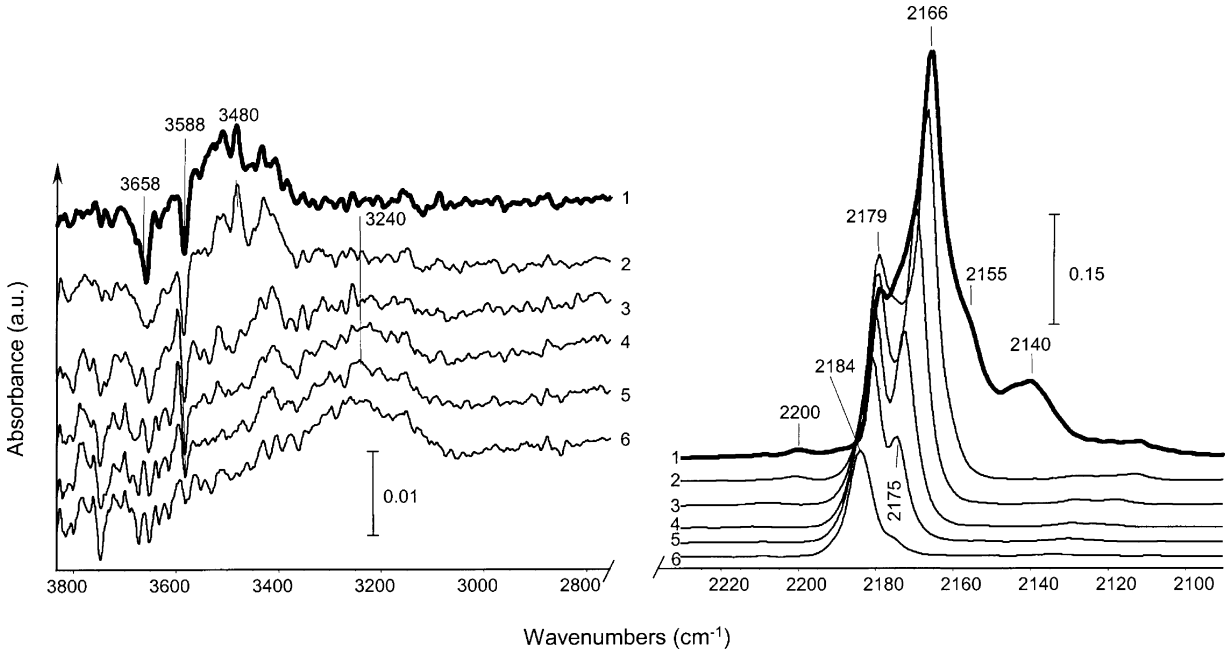

Figure 4. FTIR spectra of CO adsorbed at 77 K on $LaCl_3$ pretreated at 820 K: 1, 10.6 mbar CO in equilibrium; 2, evacuation of gas-phase CO to 1.3×10^{-4} mbar; 3, evacuation for 3 min at 1.3×10^{-4} mbar; 4, evacuation for 7 min at 1.3×10^{-5} mbar; 5, evacuation for 10 min at 1.3×10^{-5} mbar; and 6, evacuation for 20 min at 1.3×10^{-5} mbar. Spectrum before CO adsorption was subtracted.

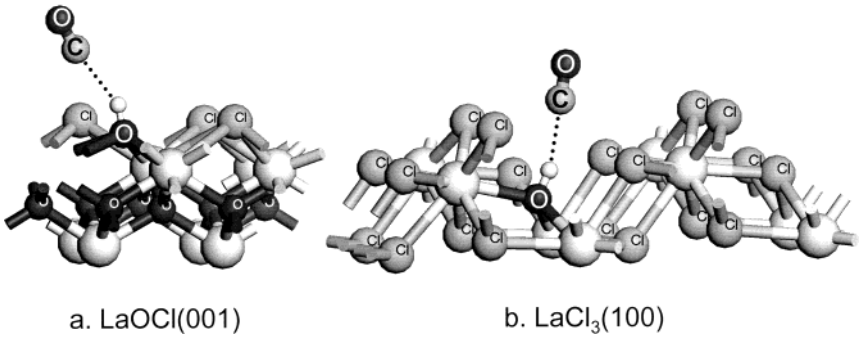

Figure 5. CO adsorption on Brønsted acid sites of model surfaces. Only top slab layers are shown for clarity.

La_2O_3, LaOCl, and $LaCl_3$ (Table 1) indicate that the strength of Brønsted acid sites increases in this order. This acidity ranking could not be confirmed computationally for La_2O_3 because a model for OH groups on La_2O_3(001) could not be generated in the same way as for the other two model surfaces. Specifically, two options were evaluated. First, when an H atom was added to a terminal lattice O, a vacancy was generated, making this model incomparable to others. And second, when H_2O was added and dissociated, with an H atom again bonding to a lattice O and with a second surface OH group being formed. Several alternative geometries for the second option were evaluated. All of them were found to be less energetically favorable (by 30−70 kJ/mol) than a molecularly adsorbed H_2O, indicating that water dissociation is endothermic. This result is in line with the conclusion of a recent spectroscopic study that a surface reconstruction is required for La_2O_3 hydration.[34]

The DFT models for CO adsorption on La^{3+} (Lewis acid) sites are shown in Figure 1. The optimized CO−La distances were 2.9−3.0 Å. The heats of adsorption decreased from −23 kJ/mol for La_2O_3 to −28 kJ/mol for a Cl-terminated LaOCl, and then decrease to −36 kJ/mol for a mixed O−Cl surface of LaOCl and, finally, to −37 kJ/mol for $LaCl_3$ (Table 2). In good agreement with the experimental values (Table 2), the calculated CO frequencies changed with the energetics, i.e., more strongly adsorbed species had vibrational modes at higher wavenumbers.

In addition to the initial models at 0.25 ML (ML = monolayer), calculations at 0.5, 0.75, and 1 ML of CO based on surface La^{3+} were performed for evaluation of coverage effects. The energy of CO adsorption was found to be constant, within 4 kJ/mol, for all models. In addition, the effect of OH presence for LaOCl and $LaCl_3$ was estimated by considering the models in Figure 5 and varying the CO coverage on La sites from 0.25 to 1 ML. The adsorption energies were again invariable with coverage and identical to those without terminal OH, within 4 kJ/mol. The only predicted change at high coverage was a band broadening of about 20 cm^{-1} due to synchronous or asynchronous vibrations of neighboring CO molecules. The ranking of Lewis acidity with CO adsorption was verified with eigenvalue estimates for the lowest unoccupied molecular orbital (LUMO). A LUMO eigenvalue in DFT corresponds to the energy change on addition of an incremental negative charge to the model and, as a result, can be used as a measure of Lewis acidity.[35] LUMO estimates were obtained with Γ-point calculations. LUMO eigenvalues, summarized in Table 2, suggest the same ranking of the Lewis acidity strength as that inferred on the basis of the CO adsorption calculations: La_2O_3 < Cl-terminated LaOCl < Cl−O-terminated LaOCl < $LaCl_3$.

The experimental frequencies of CO adsorbed at low coverage summarized in Table 2 follow the same overall Lewis acidity

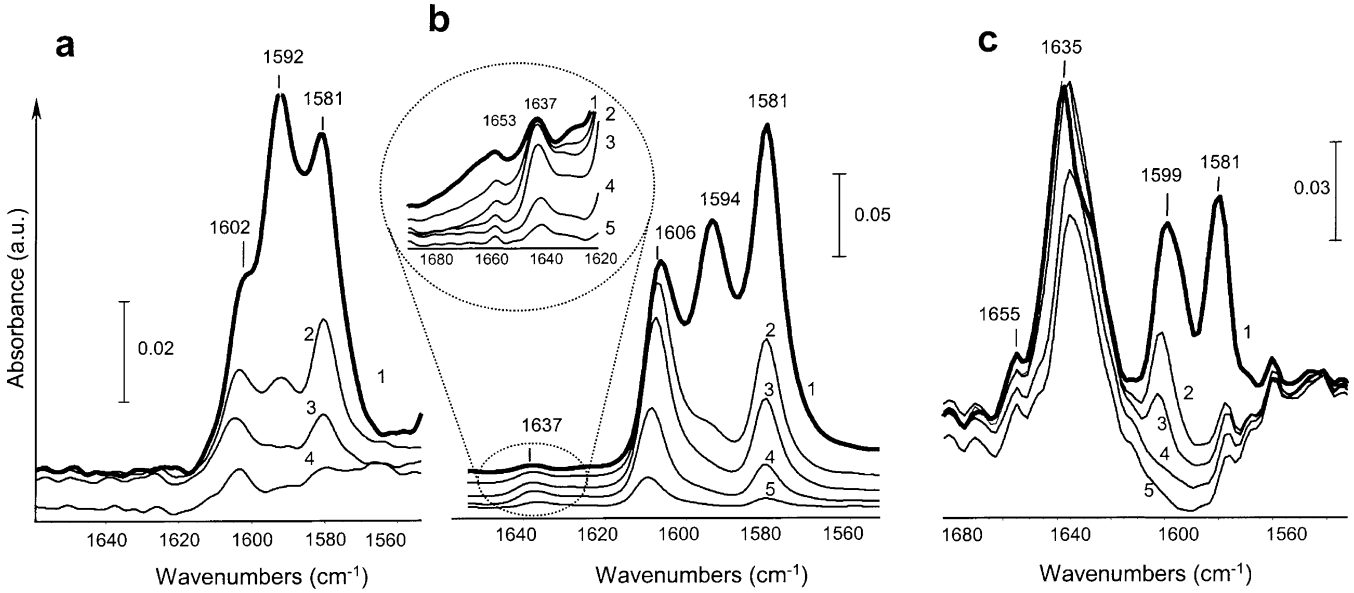

Figure 6. FTIR spectra of 2,6-dimethylpyridine (DMP) adsorbed at 300 K on a, La_2O_3; b, LaOCl; and c, $LaCl_3$: 1, 1.3 mbar in equilibrium; 2, evacuation of gas-phase DMP at RT; 3, evacuation to 1.3×10^{-3} mbar at RT; 4, evacuation at 370 K; and 5, evacuation at 470 K.

TABLE 2: Evaluation of Lewis Acid Sites on La_2O_3, LaOCl, and $LaCl_3$

	La_2O_3	LaOCl	$LaCl_3$
ν(CO) experimental at low coverage, cm^{-1}	2178	2180	2184
ν(CO) experimental at high coverage, cm^{-1}	2167, 2175(sh.)[a]	2166, 2173(sh.)	2166, 2179

		LaOCl(001)		
computational model surface	La_2O_3(001)	Cl-only	mixed O−Cl	$LaCl_3$(100)
ν(CO) calculated at 0.25 ML, cm^{-1}	2153	2157	2175	2170
ΔE for CO adsorption at 0.25 ML, kJ/mol	−23	−28	−36	−37
LUMO energy, kJ/mol. Lower energy indicates stronger Lewis acidity	−177	−208	−249	−297

[a] sh. = shoulder.

trend of La_2O_3 < LaOCl < $LaCl_3$. Specifically, the main CO band at low coverage for La_2O_3 was at 2178 cm^{-1}, whereas it was at 2180 cm^{-1} for LaOCl and 2184 cm^{-1} for $LaCl_3$ (spectra 4−6 in Figures 2−4). Similar studies of surface acidity with CO at low coverage have been reported for a number of metal oxide surfaces.[36] At high coverage, the differences between frequencies of CO adsorbed on Lewis acid sites are less pronounced (spectra 1 in Figures 2−4).

1.2. DMP and Pyridine Adsorption. DMP adsorption on the La_2O_3 sample pretreated at 1070 K gave rise to bands at 1602, 1592, and 1581 cm^{-1} (spectrum 1 in Figure 6a). The band at 1592 cm^{-1}, usually attributed to weakly bound (physisorbed) species,[21,37] disappeared first on evacuation (spectrum 3 in Figure 6a). The bands at 1602 and 1581 cm^{-1} are usually attributed to H-bonded species on hydroxy groups or to coordinated species on Lewis acid sites.[14,21,37] Sometimes, it is possible to distinguish the contribution from the two types of sites on the basis of a splitting of the band at 1602 cm^{-1} and on the basis of analysis of the ν(OH) perturbation. For La_2O_3, splitting of the 1602 cm^{-1} peak was not observed. The initial ν(OH) band for La_2O_3 at 3624 cm^{-1} (spectrum 0 in Figure 1) decreased in intensity after DMP adsorption, and a band of perturbed OH groups appeared at 3500 cm^{-1} (not shown). The bands of the free hydroxy groups were partially restored on evacuation at 370 K, indicating that most species desorbed below that temperature (spectrum 4 in Figure 6a). Therefore, H-bonded DMP definitely contributes to the bands at 1602 and 1581 cm^{-1} with a possible contribution from DMP adsorbed on Lewis acid sites.

DMP adsorption on LaOCl also produced weakly bound species with a band at 1594 cm^{-1} (spectrum 1 in Figure 6b). However, the relative intensity of this band was lower compared with those of the bands at 1606 and 1581 cm^{-1}, indicating a higher concentration of species adsorbed on Lewis acid sites and H-bonded to OH groups. The shift of the band position from 1602 cm^{-1} for La_2O_3 to 1606 cm^{-1} for LaOCl indicates stronger bonding for the latter and, correspondingly, higher acid strength of DMP adsorption sites. The perturbed hydroxy groups were not detected after evacuation at 470 K, and therefore, the bands at 1606 and 1581 cm^{-1} in spectrum 5 of Figure 6b can be attributed exclusively to species on Lewis acid sites. Compared to the spectrum of DMP on La_2O_3 in Figure 6a, the LaOCl spectra in Figure 6b had additional bands at 1653 and 1637 cm^{-1}, which are indicative of protonated $DMPH^+$ species. Although the intensities of these bands were small, their presence provided further evidence for stronger Brønsted acidity of LaOCl relative to La_2O_3.

The intensities of the bands at 1655 and 1635 cm^{-1} were considerably higher for $LaCl_3$, as shown in Figure 6c. In addition, perturbation of OH groups and a spectral depression in the CH−NH vibrational region (not shown) confirms the formation of protonated DMP ($DMPH^+$) species. The band at 1635 cm^{-1} was dominating, and its intensity did not change significantly upon evacuation at RT (spectra 1−3 in Figure 6c). The results, therefore, indicate that the concentration of Brønsted acid sites capable of protonating DMP was higher on $LaCl_3$ than on the other two materials investigated here. We note that Figure 6 compares absorbance intensities on the basis of similar

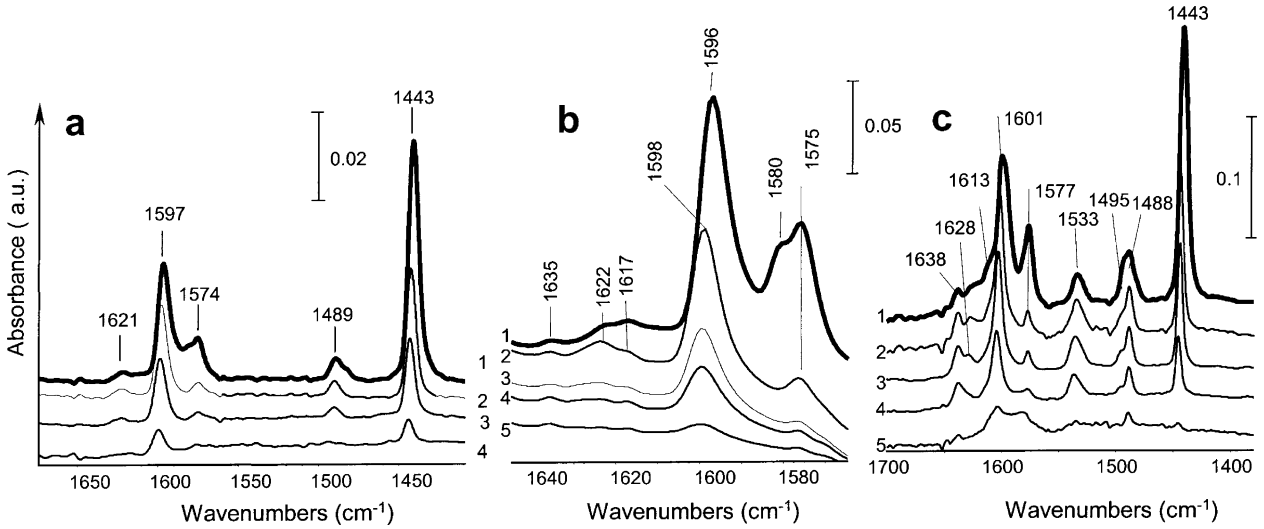

Figure 7. FTIR spectra of pyridine adsorbed at 300 K on a, La_2O_3; b, LaOCl; and c, $LaCl_3$: 1, 1.3 mbar in equilibrium; 2, evacuation of gas-phase at RT; 3, evacuation to 1.3×10^{-3} mbar at RT; 4, evacuation at 370 K; and 5, evacuation at 470 K.

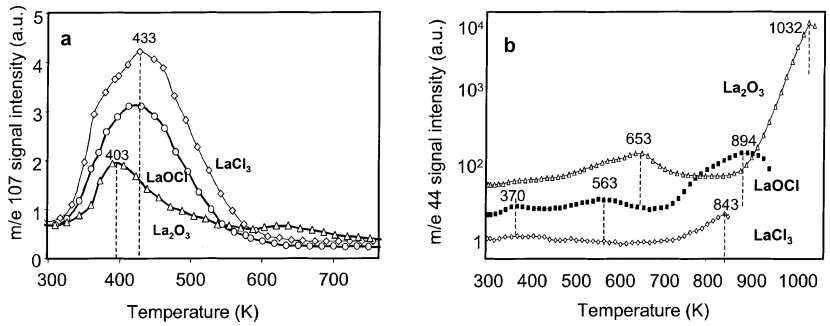

Figure 8. Temperature-programmed desorption profiles of DMP (a) and CO_2 (b) from La_2O_3, LaOCl, and $LaCl_3$

sample weights. However, the surface area of our LaOCl samples was about 40 times higher than that of La_2O_3 and $LaCl_3$, and therefore, the apparent surface concentration of DMP adsorption sites on LaOCl must have been relatively small.

Pyridine adsorption on La_2O_3 gave rise to two main peaks at 1597 and 1443 cm^{-1}, two smaller bands at 1574 and 1489 cm^{-1}, and an addition small band at 1621 cm^{-1} (Figure 7a). Similar bands were observed by Mekhemer.[30] The spectra for pyridine adsorbed on LaOCl were similar to those of pyridine adsorbed on La_2O_3, except for a week band at 1635 cm^{-1} (Figure 7b) and a stronger band at 1530 cm^{-1} (not shown); these two peaks can indicate PyH^+ species formation. The spectra for $LaCl_3$ were slightly different (i.e., the band at 1597 cm^{-1} shifted to 1601 cm^{-1} with a shoulder at 1613 cm^{-1}, the band at 1574 shifted to 1577 cm^{-1}, increasing in its relative intensity, and new bands appeared at 1638 and 1533 cm^{-1} (Figure 7c)). These results indicates moderate Brønsted acidity for LaOCl and stronger acidity for $LaCl_3$, in line with DMP measurements.

In summary, the IR measurements with DMP and pyridine confirmed the Brønsted acidity ranking on the basis of the ν(OH) shift by CO adsorption: La_2O_3 < LaOCl < $LaCl_3$. This acidity ranking was further tested by TPD of DMP (see Figure 8a). The main desorption peaks for LaOCl and $LaCl_3$ were observed at approximately 433 K. In contrast, the main desorption peak for La_2O_3 was observed already at 403 K, confirming the weaker acid strength of this material. The amount of DMP desorbed per unit weight changed according to the acidity ranking La_2O_3 < LaOCl < $LaCl_3$. Note that present pyridine and DMP adsorption results are in agreement with the spectroscopic study of chlorinated alumina, which found that pyridine could not distinguish the strength of acid sites of different samples, but DMP showed higher acid strength with the increasing extent of sample chlorination.[38]

As mentioned in the Introduction, the surface acidity of various materials has been ranked on the basis of their interactions with probe molecules. Ammonia and pyridine adsorption results were used to construct the following Lewis acidity ranking: CoO, CuO, CaO < Ni_2O_3 < MgO < NiO < ZrO_2 < Cr_2O_3 < BeO < ZnO < TiO_2 < Ga_2O_3 < Al_2O_3.[15] A comparison between our CO adsorption results (ν(CO) in Table 2) and those reported for the materials in this classification suggests that the Lewis acidity of ZrO_2[39,40] is similar to that of La_2O_3, which is lower than the acidity of LaOCl, which, in turn, is lower than the acidity of $LaCl_3$, which is comparable to that of TiO_2[41] or in summary: $ZrO_2 \approx La_2O_3$ < LaOCl < $LaCl_3$ < TiO_2.

2. Surface Basicity. CO_2 adsorption at RT on the La_2O_3 sample pretreated at 1070 K gave rise initially to three bands at 1604, 1577, and 1310 cm^{-1} and to a broad feature centered around 1442 cm^{-1} (spectrum 1 in Figure 9a). On further dosing, this feature grew into a broad massif of bands with two maxima at 1489 and 1400 cm^{-1} (spectra 2−6 in Figure 9a). In the lower-frequency region, bands were observed at 856, 850, 773, and 721 cm^{-1}. Similar spectra have previously been interpreted as initial formation bidentate (1604 and 1577 cm^{-1}) and polydentate carbonates (broad massif), which then at a higher coverage transform into bulk carbonates.[17,42,43] Our additional spectroscopic measurements with $La_2(CO_3)_3$, showing a broad massif between 1650 and 1250 cm^{-1} with two peaks at 1483 and 1390 cm^{-1}, similar to previously reported spectra,[44,45] support this interpretation.

With LaOCl, bands of adsorbed CO_2 appeared at 2357 and 2350 cm^{-1} with a shoulder at 2337 cm^{-1} (Figure 9b). These

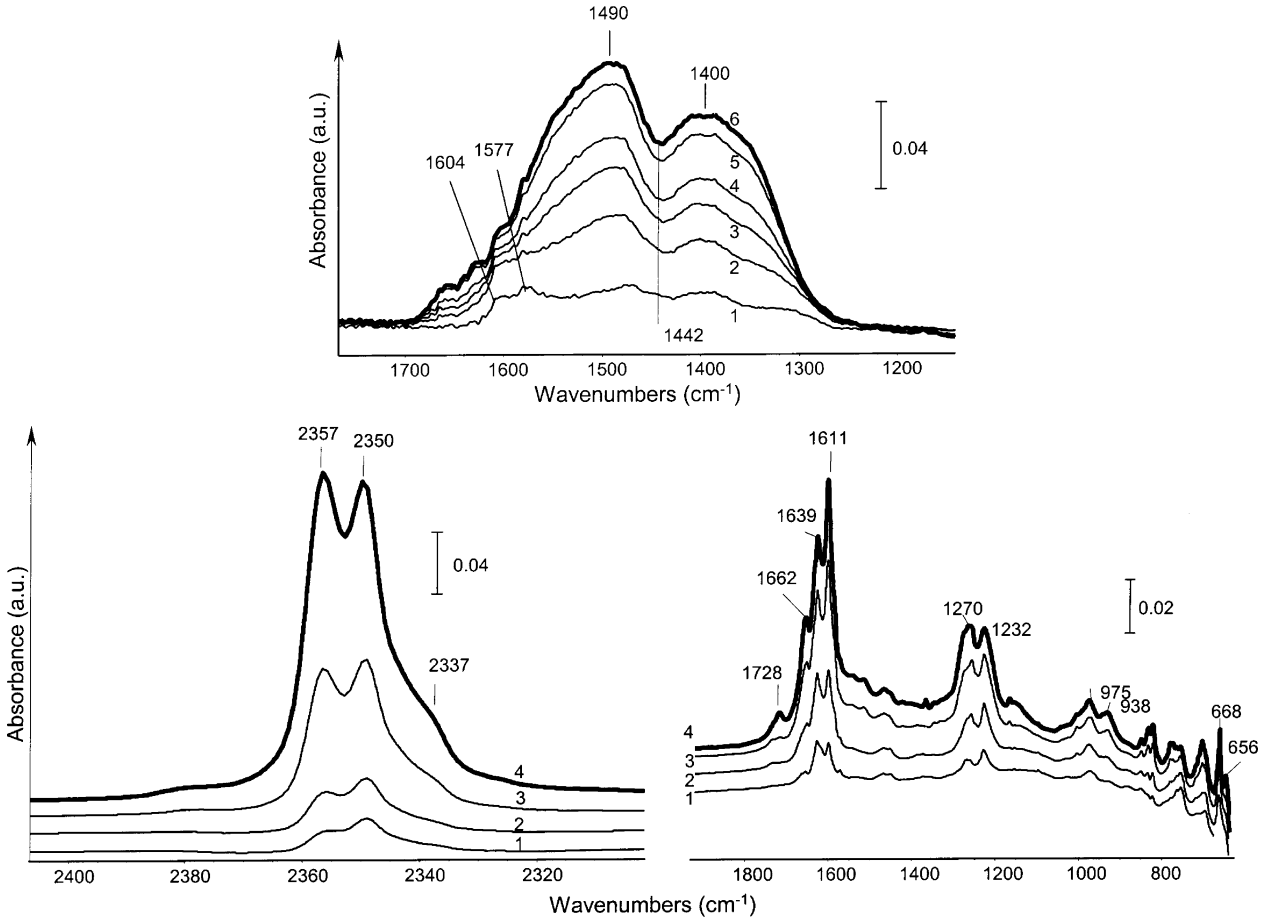

Figure 9. FTIR spectra of CO_2 adsorbed at RT on (a) La_2O_3 pretreated at 1020 K: 1, 0.1 mL dose based on assumed 10^{19} 1/m^2 site density; 2, 0.3 mL, 3−0.4 mL; 4, 0.07 mbar in equilibrium; 5, 0.7 mbar in equilibrium; and 6, 1.3 mbar in equilibrium; (b) LaOCl pretreated at 770 K at the equilibrium pressure of: 1, 0.05; 2, 0.1; 3, 0.3; and 4, 1.3 mbar.

bands have been attributed to CO_2 adsorption on Lewis acid sites.[46] In the lower-frequency region, bands were observed at 1728, 1662, 1639, 1611, 1470, 1270, 1232, 975, 938, 668, and 656 cm^{-1}. The last two frequencies are bending modes of molecular CO_2. Most of the other bands can be grouped into peak pairs that grew simultaneously (spectra 1−4 in Figure 9b): 1728 and 1662 cm^{-1}, 1639 and 1611 cm^{-1}, 1270 and 1232 cm^{-1}, and 975 and 938 cm^{-1}. These bands are consistent with those of bridged carbonate species: 1670−1620 cm^{-1} ν(C═O), 1270−1250 cm^{-1} ν_{as}(COO$^-$), and 1020−980 cm^{-1} ν_s(COO$^-$).[16,17] Therefore, the spectra of LaOCl can be interpreted as the simultaneous formation of bridged carbonate species on two different O adsorption sites. These two adsorption sites are speculatively associated with different crystal planes or with a different number of neighboring Cl and O atoms. DFT calculations suggest an assignment based on a single adsorption site model that is discussed in detail below.

Only physisorbed CO_2 was detected spectroscopically on $LaCl_3$, indicating a practical absence of terminal O atoms. This result was confirmed with TPD of CO_2 (Figure 8b), showing that the amount of CO_2 desorbed from $LaCl_3$ in a single peak at ∼843 K was orders of magnitude lower than those from La_2O_3 or LaOCl. For La_2O_3, the rate of CO_2 desorption started increasing at about 450 K and reached the first maximum at 653 K. The second, and much larger, peak was at 1032 K. The positions of these peaks are consistent with the reported thermal stability of $La_2(CO_3)_3$ based on thermogravimetric, calorimetric, spectroscopic, and elemental analyses.[44,45,47,48] The bulk carbonate phase initially converts into oxycarbonates, $La_2O_3{\cdot}xCO_2$, at about 570−675 K, which then decompose to La_2O_3 at about 770−1000 K, with the decomposition being complete around 1100 K. Therefore, the TPD results support the assignment of CO_2 spectra in Figure 9a to bulk carbonate species. For LaOCl, two small desorption peaks at 370 and 563 K followed by the main peak at 894 K were observed. An assignment of these peaks is discussed with DFT results below. In additional experiments, the elimination of carbonate species from LaOCl samples after a He treatment at 1073 K was confirmed with IR measurements.

The results of DFT calculations for CO_2 adsorption are summarized in Table 3. On La_2O_3, CO_2 is predicted to form polydentate (Figure 10a) and monodentate (Figure 10b) species. The adsorption energies for these species were all approximately 50 kJ/mol. Models of bridged and bidentate species were unstable. With both starting structures, CO_2 was optimized into the above-discussed poly- or monodentate structures. The calculated characteristic frequencies for the stable species in Table 3 agree well with experimental observations for other metal oxide surfaces.[16,17] Moreover, IR bands similar to DFT predicted frequencies for monodentate and polydentate carbonates were reported for CO_2 adsorbed on La_2O_3 calcined at 1273 K.[44]

To evaluate the sensitivity of the computed frequencies, an analysis was performed with high-coverage models where two or three CO_2 molecules were optimized on the surface of the 2 × 2 La unit cell, leading to 0.5 and 0.75 ML coverage values. The results of these calculations are presented under the "high coverage" heading in Table 3. Surface relaxation and lateral interactions between adsorbates led to geometry distortions. For example, polydentate species lost their symmetry because one

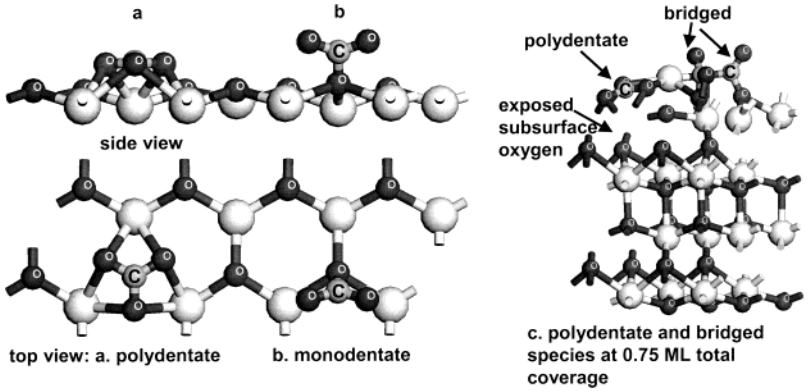

Figure 10. DFT models of carbonate species formed on CO_2 adsorption on $La_2O_3(001)$. Only top model layers are shown in (a) and (b).

TABLE 3: DFT Calculated Frequencies (cm^{-1}), C−O Bond Distances (Å), and Adsorption Energies (kJ/mol) for Species Formed on CO_2 Adsorption

Species	Schematic		Surface and coverage		
			$La_2O_3(001)$		LaOCl(001)
			0.25 ML	high coverage	0.25 ML
Polydentate		ν(C-O), cm^{-1}	n/a	1413	1434
		$\nu_{as}(CO_3)$, cm^{-1}	1401	1470	1375
		$\nu_s(CO_3)$, cm^{-1}	1037	1051	1053
		C-O bonds, Å	1.30 1.30 1.30	1.28 1.30 1.30	1.29 1.29 1.31
		ΔE ads, kJ/mol	-56		-307
Bridged type A	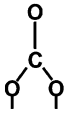	ν(C=O), cm^{-1}	converts to polydentate	1773	1724
		ν_{as}(COO), cm^{-1}		1035	1032
		ν_s(COO), cm^{-1}		970	927
		C-O bonds, Å		1.21 1.37 1.37	1.22 1.37 1.37
		ΔE ads, kJ/mol			-161
Bridged type B	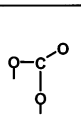	ν(C=O), cm^{-1}	converts to monodentate	1804	1756
		ν_{as}(COO), cm^{-1}		1107	1151
		ν_s(COO), cm^{-1}		898	901
		C-O bonds, Å		1.20 1.33 1.41	1.22 1.31 1.40
		ΔE ads, kJ/mol			-105
Monodentate	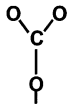	ν_{as}(COO), cm^{-1}	1691	converts to bridged	converts to polydentate
		ν_s(COO), cm^{-1}	1258		
		ν(C-O), cm^{-1}	842		
		C-O bonds, Å	1.26 1.26 1.43		
		ΔE ads, kJ/mol	-49		
Coupled bridged		ν_{as}(COO), cm^{-1}	converts to polydentate	converts to polydentate	1745, 1699
		ν_s(COO), cm^{-1}			1355, 1229
		ν(C-O), cm^{-1}			829,798
		C-O bonds, Å			1.24 1.25 1.46
		ΔE ads, kJ/mol			-153

of the C−O bonds become shorter (1.28 vs 1.30 Å), and consequently, an extra frequency was predicted at 1413 cm^{-1}. The frequencies for $\nu_{as}(CO_3)$ and $\nu_s(CO_3)$ shifted from 1401 and 1037 cm^{-1} at 0.25 ML to, respectively, 1470 and 1051 cm^{-1} at high coverage. In addition, other adsorption modes became preferable at high coverage. Monodentate species in the presence of polydentate carbonate became unstable and converted into a bridged configuration. Two bridged-geometry types were identified and classified as "A" and "B". Bridged species of type A is more symmetric, with the C−O distances for the O atoms bonding to the surface being identical. Type B species, on the contrary, is not symmetric with respect to the bonding La atoms and, consequently, all its C−O distances are not equal to one another. Figure 10c shows a representative geometry with one polydentate and two type B bridged species in the unit cell with the overall coverage of 0.75 ML, which was found to be the saturation coverage for our unit cell. This figure illustrates corrugation of the La_2O_3 surface on CO_2 adsorption and, consequently, exposure of subsurface O atoms, indicating the possibility of bulk carbonate formation on further reaction with CO_2. The DFT calculations used fixed unit-cell parameters and, therefore, could not predict the actual phase transformation.

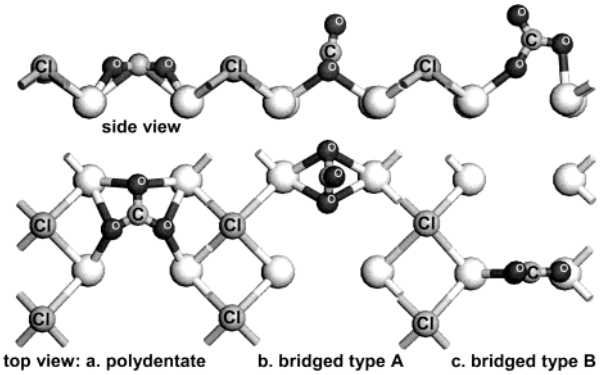

Figure 11. DFT models of carbonate species formed on CO_2 adsorption on LaOCl(001). Only top model layers are shown.

Calculations with the LaOCl model, where two surface Cl were substituted for one O atom, suggested that polydentate species were the most thermodynamically favorable structure with the adsorption energy of −307 kJ/mol (Figure 11a and Table 3). Bridged species of type A (Figure 11b) and B (Figure 10f) were less stable with energies of −161 and −105 kJ/mol, respectively. Evaluated monodentate and bidentate geometries optimized into the polydentate structure of Figure 11a. In addition, the geometries of the bridged species in Figure 11b and c were found to be sensitive to distortions: all geometries tended to converge into the polydentate structure of Figure 11a because of its high thermodynamic stability in this configuration. This result is in apparent contradiction with the experimental spectra in Figure 9b, which suggest the formation of bridged, not polydentate, carbonates. The estimated frequencies for the bridged species in Table 3 are indeed close to the experimental bands in Figure 9b.

Additional calculations were performed to address the questions of "why is polydentate carbonate not observed experimentally on LaOCl when it is predicted to be the most stable structure" and "can a difference in Cl and O adsorption-site coordination cause the experimentally observed band doubling." For the elucidation of these questions, calculations with larger (3×2) and smaller (2×1) unit cells were performed, varying the concentration of O surface sites from 0.5 to 1/6 ML. All these calculations predicted polydentate formation with the vibrational frequencies close to the ones (within 8 cm^{-1}) quoted at 0.25 ML in Table 3. Then, CO_2 adsorption on a site created by a Cl or OH vacancy on the model surface in Figure 5a was evaluated. The adsorbate on such a site was estimated to have vibrational frequencies of 1690, 1293, and 720 cm^{-1}, which

TABLE 4: Evaluation of Lewis Basicity with Proton Affinity (PA) Calculations[a]

computational model surface	La_2O_3(001)	LaOCl(001)		$LaCl_3$(100)
		Cl-only	mixed O−Cl	
ΔE for O^{2-}(surf) + H^+ = OH^- (surf) at 0.25 ML, kJ/mol	−1513		−1595	
ΔE for Cl^-(surf) + H^+ = HCl(surf) at 0.25 ML, kJ/mol		−1247	−1257	−1189

[a] For comparison, calculated and experimental[20] (in parentheses) PA of CO, pyridine, and DMP are, respectively, 618 (594), 957 (930), and 1050 (963) kJ/mol.

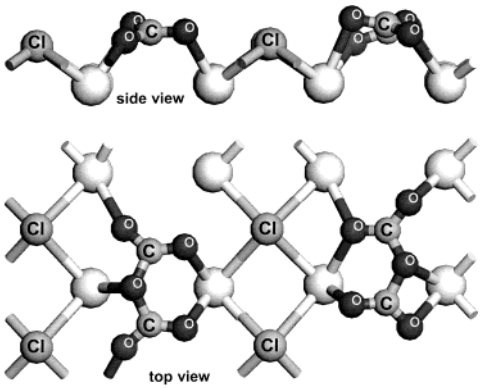

Figure 12. Two energetically equivalent geometries of coupled CO_2 adsorbate species (coupled bridge) on LaOCl(001). Each coupled pair shares a single O adsorption site. Only top model layers are shown.

are consistent with experimentally observed bands of Figure 9b. However, the presence of such surface species cannot explain the simultaneous evolution of coupled bands, even though it is plausible that these species contributed to the overall spectrum. After that, increased CO_2 coverage was modeled by bonding 2 CO_2 molecules to a single surface O site. Two energetically equivalent structures for such an arrangement are illustrated in Figure 12. In these structures, the surface O site serves as a bridge between 2 CO_2 fragments. Although these CO_2 fragments resemble polydentate species sharing one common O atom, their geometry is close to that of monodentate species on La_2O_3 (Table 3), i.e., one long C−O bond of 1.46 Å and two shorter bonds of 1.25 and 1.24 Å (the C−O bonds for the monodentate on La_2O_3 are 1.43, 1.26, and 1.26 Å). On the other hand, these CO_2 fragments are bonded to the surface through two O atoms, similar to bridged carbonates at low coverage. As a result, they can be classified as coupled bridged species, and their predicted vibrational frequencies are between those for monodentate and bridged carbonates (Table 3). Importantly, these frequencies are doubled because, for every movement of one of the CO_2 fragments, the other fragment can move symmetrically or asymmetrically. For example, for the ν_{as}(COO) mode, the symmetric movement of the coupled fragments was estimated to be at 1745 cm^{-1} and the asymmetric movement at 1699 cm^{-1}. The predicted doubled frequencies at 1745 and 1699 cm^{-1}, 1355 and 1229 cm^{-1}, and 829 and 798 cm^{-1} in Table 3 are in general, but not perfect, agreement with the experimental bands in Figure 9b at 1639 and 1611 cm^{-1}, 1270 and 1232 cm^{-1}, and 975 and 938 cm^{-1}. To evaluate the sensitivity of the calculated frequencies to geometry perturbations and types of neighboring species, additional calculations with constrained optimization and different unit-cell sizes were performed. The predicted frequencies were found to be sensitive to geometry changes. For example, changing one C−O distance from 1.46 to 1.40 Å produced a structure with noticeably different ν(C−O) at 965 and 882 cm^{-1} but with an adsorption energy only 4 kJ/mol higher. In contrast, varying the concentration of the coupled bridged species from 1/6 to 0.5 ML on the chlorinated surface, as well as changing the local surrounding from Cl to O, had little effect both on the predicted frequencies and on the adsorption energies; the results were, respectively, within 8 cm^{-1} and 10 kJ/mol.

The adsorption energy for the coupled bridged species was predicted to be −153 kJ per mol of CO_2. This implies that if one CO_2 molecule bonded to an O site and formed a bridged type A species with the binding energy of −161 kJ/mol (Table 3), a second CO_2 molecule could bond to the same site with the energy of $-153 \times 2 - (-161) = -145$ kJ/mol. If the first molecule formed a polydentate species, then the addition of the second one would be thermo-nuetral: −307 kJ/mol for polydentate versus $-153 \times 2 = -306$ kJ/mol for the coupled bridged species. The coupled bridged species would be the most abundant species if the formation of polydentate carbonates were limited kinetically. However, at elevated temperatures, this limitation should disappear and a conversion to polydentate carbonates should take place. The CO_2 TPD profile for LaOCl in Figure 8b appears to be consistent with this hypothesis. If predominantly coupled bridged species are formed at RT, they would stay on the surface when physisorbed species desorb at about 370 K. Then, at the temperature of the second peak, at about 563 K, the coupled bridge species would decompose into gas-phase CO_2 and polydentate carbonates. And finally, the last desorption peak at 894 K can be assigned to decomposition of polydentate carbonates. If the concentration of O surface sites was constant, the second desorption peak would be similar to the third one, i.e., a half of adsorbed CO_2 would desorb on the formation of polydentate carbonates and the other half when they decompose. Our reported chlorination experiments, however, demonstrated a facile exchange between surface Cl atoms and bulk O atoms at elevated temperatures.[10,12] As a result, migration of O atoms from the bulk to the surface can explain the conversion of the majority of adsorbed CO_2 into polydentate carbonates and, accordingly, the main desorption peak occurring at the temperature of polydentate decomposition.

The basicity of different materials can usually be compared on the basis of interactions with CO_2. In the case of La_2O_3 and LaOCl, the analysis is complicated by the formation of apparently different surface species. Whereas bulk carbonates were formed with La_2O_3, the structure of LaOCl (Figure 1b) with Cl layers prevented a phase transformation at moderate temperatures when surface-to-bulk anion diffusion was limited. Nevertheless, La_2O_3 appeared to be more reactive, and a higher reactivity is usually linked to stronger basicity. To elucidate this conclusion and to include $LaCl_3$ in the basicity comparison, proton affinity (PA) calculations were performed for O and Cl surface sites, and the results are presented in Table 4. These calculations are different from the proton-abstraction calculations in Table 1, in which H^+ was removed from the model and the remaining unit cell got a formal charge of −1. In this case, H^+ was added to a basic site, and the whole unit cell got a formal charge of +1. The computational results show, for the mixed O−Cl-terminated LaOCl surface, the basic strength of O

adsorption sites can be comparable and even higher (PA of 1595 kJ/mol) than that of O sites on La_2O_3 (1513 kJ/mol). We are currently testing this hypothesis of the existence of highly basic sites on LaOCl with TPR experiments, comparing the relative catalytic activities of La_2O_3 and LaOCl surfaces. The DFT results for protonation of surface Cl sites in Table 4 showed that these sites were more basic on LaOCl (PA of 1247 kJ/mol) than those on $LaCl_3$ (1189 kJ/mol). In addition, Cl sites on the mixed O−Cl-terminated LaOCl were slightly more basic (PA of 1257 kJ/mol) than those on Cl-only terminated LaOCl (1247 kJ/mol).

Conclusions

1. FTIR measurements indicate that at low surface coverage at 77 K, CO adsorbs on Lewis acid sites of La_2O_3, LaOCl, and $LaCl_3$. The frequency shift for adsorbed CO indicates that Lewis acid strength increases with the extent of chlorination: La_2O_3 < LaOCl < $LaCl_3$. DFT calculations suggest that Lewis acid sites are associated with La^{3+}, that the saturation coverage for these sites is 1 ML, and that the adsorption energetics do not vary with coverage. The calculations also confirm the trend of CO vibrational frequency shifting to higher wavenumbers with increasing chlorination extent. Calculated estimates for CO adsorption energies and for LUMO energies confirm the Lewis acidity ranking.

2. Shifts of OH vibrational frequencies to lower wavenumbers at high CO coverage at 77 K provide evidence for adsorption on hydroxy groups, suggesting that the hydrogen-bond strength increases in the sequence La_2O_3 < LaOCl < $LaCl_3$, in agreement with the sequence the strength of Lewis acid sites. DFT calculations confirm that CO is H-bonded to OH groups. Computed shifts for ν(OH) on CO adsorption and proton abstraction energies confirm that OH groups are more strongly acidic on $LaCl_3$ than on LaOCl.

3. Stronger basic molecules, such as pyridine and DMP, adsorb primarily on Brønsted acid sites and are protonated upon adsorption on LaOCl and $LaCl_3$. The thermal stability, as probed with TPD, confirms the same acid strength ranking.

4. IR spectra of CO_2 adsorbed on La_2O_3 at RT indicate the formation of polydentate and bulk carbonates. High-coverage spectra are consistent with those of bulk $La_2(CO_3)_3$. A detailed analysis of CO_2 adsorbates with estimates of vibrational modes is provided on the basis of DFT calculations. For La_2O_3, the calculations predict the formation of monodentate and polydentate species at low coverage. At high coverage, the calculations predict surface corrugation and, consequently, exposure of bulk O atoms, suggesting bulk carbonate formation on further reaction with CO_2. The thermal stability of the carbonates is in line with these calculations, showing that, indeed, $La_2(CO_3)_3$ is formed at a high coverage of CO_2.

5. IR spectra of CO_2 adsorbed on LaOCl at RT indicate the formation of bridged carbonates. DFT calculations show that the spectra are consistent with the formation of coupled bridged species sharing a single O adsorption site. CO_2 evolution from LaOCl in TPD experiments can be interpreted in terms of conversion of coupled bridged species into polydentate carbonates and the eventual decomposition of the latter at elevated temperatures. The amount of CO_2 evolved from $LaCl_3$ in TPD experiments was negligibly small. In agreement with this, adsorbed CO_2 was not detected spectroscopically, suggesting a virtual absence of lattice O adsorption sites.

6. More facile formation of polydentate carbonates and their higher decomposition temperature suggest that lattice O sites on La_2O_3 are more basic than on LaOCl. The basicity comparison, however, is confounded by the formation of different carbonate types on these two materials. Proton-affinity calculations suggest that lattice O sites may exist on a mixed Cl−O surface of LaOCl that are more basic than those on La_2O_3. The calculations also indicate that Cl sites are less basic on $LaCl_3$ than on LaOCl.

Acknowledgment. This work has been supported by The Dow Chemical Company, a Van Gogh grant of NWO for cooperation with Caen University, and an NWO/CW-VICI grant. We also thank the following people at The Dow Chemical Company for useful discussions: R. Gulotty, M. Jones, A. Schweizer, M. Olken, B. Bardin, M. McAdon, P. Margl, and M. Tirtowidjojo. We also gratefully acknowledge the contribution of R. Lee in the development of the slab surface models used in DFT calculations.

Supporting Information Available: Crystallographic information files (CIF) for structures in Figures 1, 5, 10−12. This material is available free of charge via the Internet at http://pubs.acs.org.

References and Notes

(1) Lunsford, J. H. *Angew. Chem., Int. Ed. Engl.* **1995**, *34*, 970.
(2) Campbell, K. D.; Lunsford, J. H. *J. Phys. Chem.* **1988**, *92*, 5792.
(3) Kaddouri, A. H.; De Blasio, N.; Del Rosso, R. *React. Kinet. Catal. Lett.* **2001**, *72*, 309.
(4) Au, C. T.; He, H.; Lai, S. Y.; Ng, C. F. *Appl. Catal., A* **1997**, *159*, 133.
(5) Sugiyama, S.; Sogabe, K.; Miyamoto, T.; Hayashi, H.; Moffat, J. B. *Catal. Lett.* **1996**, *42*, 127.
(6) Ciambelli, P.; Lisi, L.; Pirone, R.; Ruoppolo, G.; Russo, G. *Catal. Today* **2000**, *61*, 317.
(7) Schweizer, A. E.; Jones, M. E.; Hickman, D. A. US 6452058 B1, 2002
(8) Henley, J. P.; Jones, M. E.; Hickman, D. A.; Marshall, K. A.; Reed, D. J.; Clarke, W. D.; Olken, M. M.; Walko, L. E. WO 2001038274 A1, 2001.
(9) Jones, M. E.; Henley, J. P.; Hickman, D. A.; Marshall, K. A.; Reed, D. J.; Clarke, W. D.; Olken, M. M.; Walko, L. E. WO 2001038272 A1, 2001.
(10) Van der Avert, P.; Manoilova, O.; Podkolzin, S. G.; Weckhuysen, B. M. *Chem. Eur. J.* **2004**, *10*, 1637.
(11) Weckhuysen, B. M. *Phys. Chem. Chem. Phys.* **2003**, *5*, 4351.
(12) Van der Avert, P.; Weckhuysen, B. M. *Angew. Chem., Int. Ed.* **2002**, *41*, 4730.
(13) Weckhuysen, B. M.; Rosynek, M. P.; Lunsford, J. H. *Phys. Chem. Chem. Phys.* **1999**, *1*, 3157.
(14) Busca, G. *Phys. Chem. Chem. Phys.* **1999**, *1*, 723.
(15) Tret′yakov, N. E.; Filimonov, V. N. *Kinet. Katal.* **1973**, *14*, 803.
(16) Davydov, A. *Molecular spectroscopy of oxide catalyst surfaces*; Wiley: London, 2003.
(17) Lavalley, J. C. *Catal. Today* **1996**, *27*, 377.
(18) Zaki, M. I.; Vielhaber, B.; Knoezinger, H. *J. Phys. Chem.* **1986**, *90*, 3176.
(19) Cairon, O.; Chevreau, T.; Lavalley, J.-C. *J. Chem. Soc., Faraday Trans.* **1998**, *94*, 3039.
(20) Hunter, E. P. L.; Lias, S. G. *J. Phys. Chem. Ref. Data* **1998**, *27*, 413.
(21) Corma, A.; Rodellas, C.; Fornes, V. *J. Catal.* **1984**, *88*, 374.
(22) Lahousse, C.; Aboulayt, A.; Mauge, F.; Bachelier, J.; Lavalley, J. C. *J. Mol. Catal.* **1993**, *84*, 283.
(23) Jacobs, P. A.; Heylen, C. F. *J. Catal.* **1974**, *34*, 267.
(24) Matulewicz, E. R. A.; Kerkhof, F. P. J. M.; Moulijn, J. A.; Reitsma, H. J. *J. Colloid Interface Sci.* **1980**, *77*, 110.
(25) Babaeva, M. A.; Bystrov, D. S.; Kovalgin, A. Yu.; Tsyganenko, A. A. *J. Catal.* **1990**, *123*, 396.
(26) Zhou, W.; Jefferson, D. A.; Liang, W. Y. *Surf. Sci.* **1989**, *209*, 444.
(27) Le Van, T.; Che, M.; Kermarec, M.; Louis, C.; Tatiboutet, J. M. *Catal. Lett.* **1990**, *6*, 395.
(28) Hussein, G. A. M.; Gates, B. C. *J. Chem. Soc., Faraday Trans.* **1996**, *92*, 2425.
(29) Palmer, M. S.; Neurock, M.; Olken, M. M. *J. Am. Chem. Soc.* **2002**, *124*, 8452.
(30) Mekhemer, G. A. H. *Phys. Chem. Chem. Phys.* **2002**, *4*, 5400.

(31) Tsyganenko, A. A.; Lamotte, J.; Gallas, J. P.; Lavalley, J. C. *J. Phys. Chem.* **1989**, *93*, 4179.
(32) Bardin, B. B.; Bordawekar, S. V.; Neurock, M.; Davis, R. J. *J. Phys. Chem. B* **1998**, *102*, 10817.
(33) van Santen, R. A. *Catal. Today* **1997**, *38*, 377.
(34) Paulidou, A.; Nix, R. M. *Surf. Sci.* **2000**, *470*, L104.
(35) Kawakami, H.; Yoshida, S. *J. Chem. Soc., Faraday Trans. 2* **1985**, *81*, 1129.
(36) Travert, A.; Manoilova, O. V.; Tsyganenko, A. A.; Mauge, F.; Lavalley, J. C. *J. Phys. Chem. B* **2002**, *106*, 1350.
(37) Petit, C.; Mauge, F.; Lavalley, J. C. *Stud. Surf. Sci. Catal.* **1997**, *106*, 157.
(38) Clet, G.; Goupil, J. M.; Cornet, D. *Bull. Soc. Chim. Fr.* **1997**, *134*, 223.
(39) Hertl, W. *Langmuir* **1989**, *5*, 96.
(40) Kondo, J.; Abe, H.; Sakata, Y.; Maruya, K.; Domen, K.; Onishi, T. *J. Chem. Soc., Faraday Trans. 1* **1988**, *84*, 511.
(41) Tsyganenko, A. A.; Filimonov, V. N. *J. Mol. Struct.* **1973**, *19*, 579.
(42) Bernal, S.; Botana, F. J.; Garcia, R.; Rodriguez-Izquierdo, J. M. *React. Solid.* **1987**, *4*, 23.
(43) Bernal, S.; Diaz, J. A.; Garcia, R.; Rodriguez-Izquierdo, J. M. *J. Mater. Sci.* **1985**, *20*, 537.
(44) Klingenberg, B.; Vannice, M. A. *Chem. Mater.* **1996**, *8*, 2755.
(45) Jeevanandam, P.; Koltypin, Yu.; Palchik, O.; Gedanken, A. *J. Mater. Chem.* **2001**, *11*, 869.
(46) Daturi, M.; Binet, C.; Lavalley, J. C.; Blanchard, G. *Surf. Interface Anal.* **2000**, *30*, 273.
(47) Sklyarenko, Yu. S.; Sklyarenko, I. S.; Chubukova, T. M. *Zh. Anal. Khim.* **1961**, *16*, 417.
(48) Ambrozhii, M. N.; Luchnikova, E. F.; Sidorova, M. I. *Zh. Neorg. Khim.* **1960**, *5*, 366.